Effects of Enhanced Sodium Currents in Mathematical Model of Heterogeneous Myocardium

Nathalie Vikulova[1,2], Anastasia Khokhlova[1,2], Leonid B Katsnelson[1,2], Olga Solovyova[1,2,3]

[1]Institute of Immunology and Physiology, Russian Academy of Sciences
[2]Ural Federal University, Yekaterinburg, Russia
[3]Institute of Mathematics and Mechanics, Russian Academy of Sciences

Abstract

Cardiac arrhythmias and long QT syndrome may be associated with increased sodium currents. Possible effects of enhanced function of sodium channels on the transmural gradient in the electrical and mechanical properties of myocardium have not been sufficiently studied. We used our cellular mathematical models to investigate effects of an increased late sodium current on the electromechanical coupling in single subendocardial and subepicardial cells and in a strand of transmurally heterogeneous myocardium. Modeling results predicted that subepicardial cells are more vulnerable to rhythm disturbances than single subendocardial cells under these pathological conditions. Within the transmurally heterogeneous strand, mechanical and electrical interactions between such abnormal cells affected the patterns of electromechanical disturbances as compared to the single cells. This allowed myocardium to contract even in those conditions where single EPI cells lost contractility.

1. Introduction

Na^+ currents in cardiomyocytes may be altered in pathology (ischemia, for instance [1]). Mutations in the SCN5A gene encoding cardiac Na^+ channels may cause the long QT interval syndrome [2] and trigger arrhythmia caused by elevation of intracellular Na^+ and subsequent cellular and sarcoplasmic reticulum (SR) Ca^{2+} overload. Sakmann et al. reported that persistent (late) Na^+ current which is activated during the AP plateau, differ in cardiomyocytes from transmural layers of guinea pig ventricle [3]. It would be expected that electrophysiological and mechanical activity of subendocardial (ENDO) and subepicardial (EPI) cells might be different under enhanced Na^+ currents. We utilized our mathematical models to study effects of enhanced Na^+ currents on electromechanical behavior of cells from different layers of left ventricular (LV) wall.

2. Methods

2.1. Mathematical models

We used our EPI and ENDO cell models, which account for transmural differences in ionic currents and myofilament contractile mechanisms between the cells [4]. These models are based on the "Ekaterinburg-Oxford" (EO) model of guinea pig single cardiomyocyte [6]. The cellular models allow one to reproduce specific features of the ionic mechanisms of action potential (AP) generation, intracellular Ca^{2+} dynamics and mechanical activity for each of cellular subtypes. The EPI model produces shorter AP, faster Ca^{2+} transient and faster contractions as compared to the ENDO model in consistency with the experimental data [4].

To simulate behavior of a heterogeneous muscle strand we used a 1D continuous model of heterogeneous myocardial tissue comprising mechanically and electrically interacting cardiomyocytes [7]. In our simulations, one third of the tissue strand consisted of the ENDO models, one third – of the EPI models. In the middle segment, parameters of the models were gradually distributed between ENDO and EPI values. In-series coupling between the cells of different transmural subtypes in the 1D tissue may reflect anatomical data showing that myocardial fiber continuously moves helically through the ventricular wall from the base to apex and from the subendocardium to subepicardium [5]. We simulated isometric contractions of a strand (12.7 mm long) being 27% pre-stretched from the slack length to achieve initial sarcomere lengths of 2.0 μm within the tissue. Depolarization wave was initiated at the ENDO edge of the tissue at 1 Hz pacing rate, and spread out at a velocity of ≈ 0.6 m/s along the strand from the ENDO segment towards the EPI one. AP generation and

mechanical activity in interacting cells within the strand were regulated by the mechanisms of electro-mechanical coupling on the cellular and tissue levels [7].

The Euler numerical integration algorithm with a time step of $\Delta t = 10^{-5}$ s was used to solve ODE system for cellular models. For the 1D model discretization, we used a spatial step of $\Delta x = 0.25$ mm. Boundary problem for the cable reaction-diffusion equation was solved by Godunov splitting method [7, 8]. Local deformations of each cell obtained from the cellular models were used for numerical solution of equations describing global deformations of the strand [7]. All simulation results are shown for the steady state contractions.

2.2. Simulation of Enhanced Sodium Currents

Under control conditions maximum conductivity g_{pNa} of persistent Na^+ current (I_{pNa}) was set to 5.2 μS in the ENDO model vs. 4.5 μS in the EPI model to reflect transmural difference in I_{pNa} density observed in ENDO and EPI ventricular cardiomyocytes [9].

To simulate "moderate" increase in I_{pNa} we increased g_{pNa} twofold as compared to the control. This did not result in rhythm disturbances in single ENDO and EPI models. To simulate "strong" increase in I_{pNa} we performed step-by-step increase in g_{pNa} to achieve arrhythmic activity in ENDO and EPI cells.

3. Results

3.1. Control twitches

Under control conditions, action potential duration (APD) of the single ENDO and EPI cells was 260 ms and 202 ms, respectively. Within the heterogeneous tissue, in which cells electrically and mechanically interact, pre-existed transmural difference in the electrical and mechanical characteristics of the cells was modulated. In steady-state contractions, APD increased in both ENDO and EPI segments of the strand: 269 ms at the ENDO edge and 212 ms at the EPI edge.

The dispersion of repolarization (DR, calculated as the difference between the times to reach 90% of repolarization in the strand edges) was -37 ms, where minus means that first stimulated ENDO cells repolarized later than last stimulated EPI cells, corresponding to experimental data *in vivo* showing opposite direction of depolarization and repolarization waves [10].

3.2. "Moderate" increase in I_{pNa}

Figure 1 compares electromechanical activity of simulated single ENDO (left panels) and EPI (right panels) cells under "moderate" increase in maximum conductivity g_{pNa} with that of cells in control conditions. Two times increase in g_{pNa} resulted in a growth of maximum amplitude of I_{pNa} up to 0.15 nA (197% of the control value) in the ENDO model and up to 0.13 nA (198% of the control value) in the EPI model (Fig. 1, bottom panels). Additional Na^+ entered through the Na^+ channels from cycle to cycle resulted in small rise of intracellular Na^+ concentration ($[Na^+]_i$) at the steady state. The ENDO model demonstrated 4% increase in diastolic $[Na^+]_i$ *vs.* 2% increase in the EPI model. Intracellular Na^+ accumulation was accompanied with an increase in the intracellular Ca^{2+} loading due to Na^+-Ca^{2+} exchange acceleration.

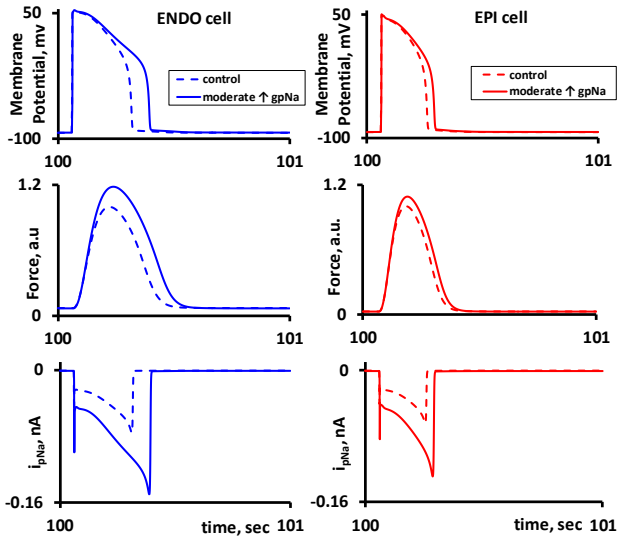

Figure 1. Model predictions on the membrane potential (*top*), isometric force (*middle*) and I_{pNa} (*bottom*) time course in single ENDO and EPI cells under "moderate" increase of I_{pNa} (*solid lines*) compared to the control twitches (*dashed lines*).

These changes resulted in the AP plateau prolongation in both type cells. The ENDO model demonstrated more pronounced increase in APD than the EPI one (Fig. 1, top panels), which is in good agreement with experimental data from canine ventricle [11]. APD in the ENDO model increased to 335 ms (29% increment above the control APD) and APD in the EPI model increased to 232 ms (15% increment above the control APD). Intracellular Ca^{2+} accumulation led to an inotropic effect, with an increase in the amplitude of isometric force (Fig. 1, middle panels) in ENDO and EPI cells by 18% and 9% compared with control values. Time to peak force increased from 163 ms to 179 ms for the ENDO model and from 123 ms to 131 ms for the EPI model.

3.3. "Strong" increase in I_{pNa}

Figure 2 shows simulation of the electrical and

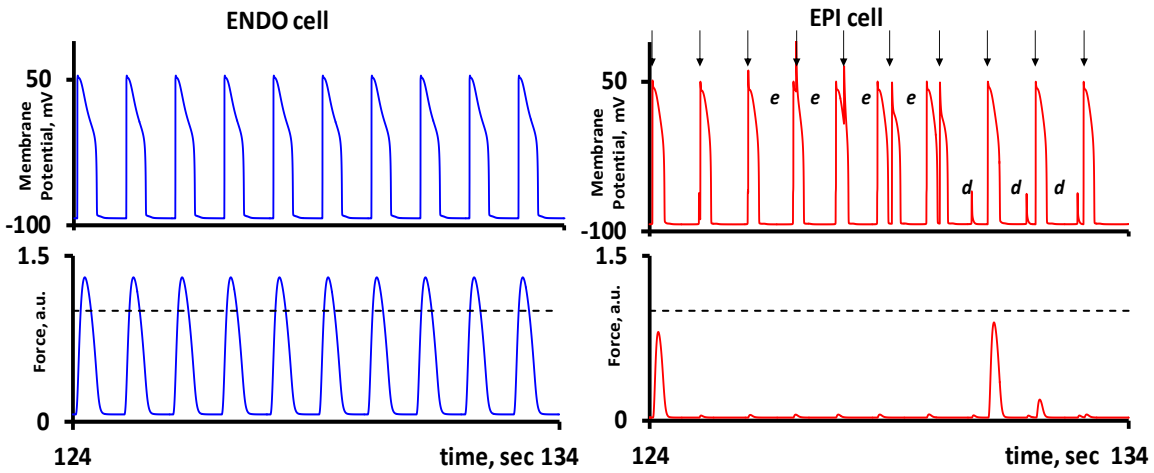

Figure 2. Membrane potential (*top*) and isometric force (*bottom*) in ENDO and EPI models under 2.5-fold increase of I_{pNa}. Arrows show regular stimuli. Delayed afterdepolarizations and extra APs are labelled "d" and "e", respectively. Isometric force is normalized by the maximum of isometric force in control conditions, which level is shown by dashed lines.

mechanical activity in the ENDO and EPI cells under 2.5-fold increase in g_{pNa}. For the EPI model, such a "strong" increase in I_{pNa} resulted in delayed afterdepolarizations (DADs, labelled "d") and extra APs (labelled "e") prior to regular stimuli (marked by arrows). Rhythm disturbances observed in the model arose due to the threshold Ca^{2+} overload, which resulted from an enhanced Ca^{2+} inflow via the Na^+–Ca^{2+} exchanger in response to the significant increase in intracellular Na^+. Mechanisms underlying such kind of rhythm disturbances we have earlier analyzed in detail within the model elsewhere [6]. These rhythm disturbances caused complete contraction failure of the EPI model (see Fig. 2).

For the ENDO model, such increase in I_{pNa} didn't result in the arrhythmic activity, but led to subsequent increase in APD up to 396 ms (152% of the control APD) and further growth (by 30% of the control value) of the isometric force amplitude (Fig. 2, left panels).

Rhythm disturbances arose in the ENDO model when g_{pNa} was increased more than 3 times over the control value. Figure 3 demonstrates first 100 cycles of the ENDO cell contractions after 3.25-fold increase in g_{pNa}. The first 25 cycles were characterized by prolonged APs (three times longer than the control one) and by irregular amplitude of isometric force, which was smaller than in control conditions. The next 10 cycles appeared to be complex interchange of regular stimuli and multiple early afterdepolarizations (EADs) making the cell incompletely repolarized. Total contractility loss was seen during this period. For the next 30 seconds, the ENDO model produced DADs and extra APs, which were accompanied with alternating isometric twitches of high amplitude interlaced with low or absent contractions. The last cycles up to 100 s demonstrated transition to the steady state with APD = 485 ms, which is 186% of the control value and with isometric force amplitude of 145% of force amplitude in control conditions.

More than 3.5-fold increase in g_{pNa} for the ENDO model led to the total loss of contractility and to membrane potential oscillations typical to EADs.

ENDO and EPI models with 2.5-fold increase in g_{pNa} ("strong" increase for the EPI model) were examined within the 1D tissue model. Figure 4 shows that interacting cells in the 1D tissue strand demonstrated different electromechanical behavior than isolated cells under enhanced I_{pNa} (compare with Fig. 2). In the strand, APDs varied from 449 ms to 283 ms within the ENDO segment and from 312 ms to 232 ms within the EPI segment. In contrast to the single EPI model, less frequent

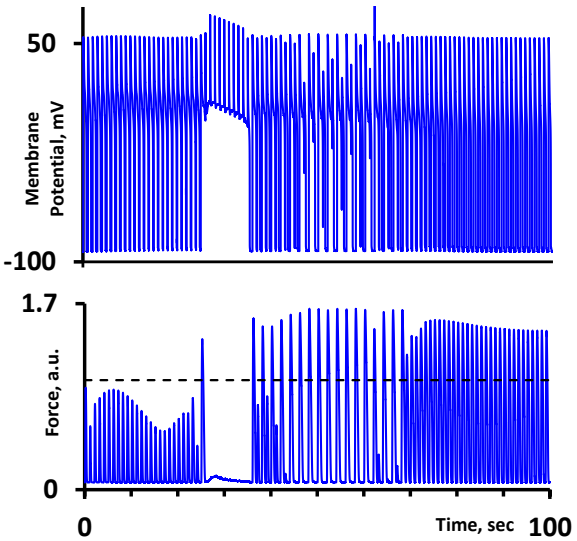

Figure 3. Membrane potential (*top*) and isometric force (*bottom*) tracings in the ENDO model during first 100 seconds of g_{pNa} 'strong' 3.25-fold increase. Periods of rhythm disturbances and disrupted contractility followed by steady state APs generation and force production.

DADs and absent extra APs were observed in EPI cells within the strand (Fig. 3, top outlined). Nevertheless, these abnormalities resulted in the loss of contractility in the EPI segment. Middle panel of Figure 4 demonstrates dynamic strain of the cells during strand contractions. During control contractions, all cells of the strand actively shortened, when excitation wave reach them (dotted lines), whereas under high g_{pNa}, EPI cells were passively stretched by actively shortening cells from the ENDO and intermediate segments during each cycle (Fig. 4, middle, dotted lines). This pathological deformation pattern, when EPI cells have lost their contractility, resulted in a significant decrease in the isometric force peak generated by the strand (Fig. 4, bottom, solid lines).

Electromechanical interaction between the cells in the strand induced beat-to-beat changes in APDs, which was revealed in a sufficient increase in the DR compared with the control one (Fig. 4, top) that may produce a long QT interval in LV.

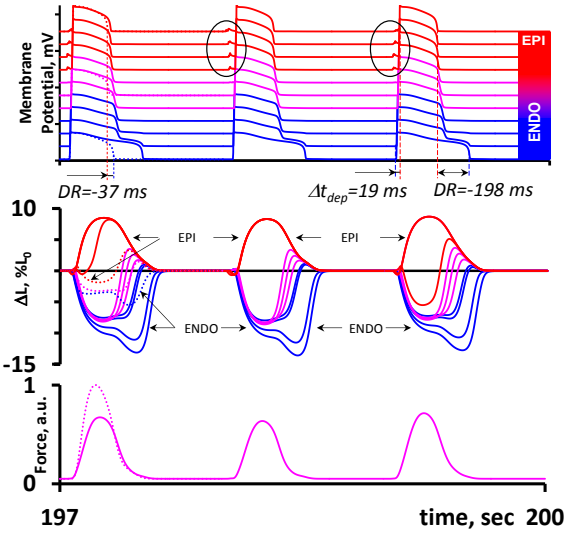

Figure 4. Effects of the 2.5-fold increase in the I_{pNa} ("strong" effect on the EPI cells) in the 1D tissue strand model. *Top*: membrane potential in cells along the strand (excitation spreads from the bottom ENDO to the top EPI segments with delay Δt_{dep}). DADs in the EPI segments are outlined. *Middle*: regional cell deformations (ΔL, % of the initial cell length Lo). *Bottom*: isometric force generated by the strand (normalized to the control peak force). Dotted lines show the reference values in the control conditions for the strand.

4. Conclusions

We showed that enhanced I_{pNa} was able to induce abnormalities in the activity of both ENDO and EPI cells, but scenarios of rhythm disturbances were different. We found that the single EPI cells were more vulnerable to rhythm disturbances compared with the single ENDO cells. Electrical and mechanical interactions between cardiomyocytes within a heterogeneous tissue was able to preserve from the total loss of the overall contraction under increased I_{pNa}.

Acknowledgements

Single cell simulations are supported by Russian Basic Research Foundation (#14-01-31134). The 1D model simulations are supported by the Russian Science Foundation (#14-35-00005).

References

[1]. Ju YK, Saint DA, Gage PW. Hypoxia increases persistent sodium current in rat ventricular myocytes. J Physiol 1996; 497(2): 337-347.

[2]. Maltsev VA, Undrovinas A. Late sodium current in failing heart: Friend or foe? Prog Biophys Mol Biol 2008; 96:421-451.

[3]. Sakmann BF, Spindler AJ, Bryant SM, et al. Distribution of a persistent sodium current across the ventricular wall in guinea pigs. Circ Res 2000; 87(10): 910-914.

[4]. Vasilyeva AD, Solovyeva OE. Electromechanical coupling in cardiomyocytes from transmural layers of guinea pig left ventricle. Biophysics 2012; 57:852-9.

[5]. Sengupta PP, Krishnamoorthy VK, Korinek J, et al. Left ventricular form and function revisited: applied translational science to cardiovascular ultrasound imaging. J Am Soc Echocardiogr 2007; 20, 539-551.

[6]. Sulman T, Katsnelson LB, Solovyova O, Markhasin VS. Mathematical modeling of mechanically modulated rhythm disturbances in homogeneous and heterogeneous myocardium with attenuated activity of Na^+-K^+ pump. Bull Math Biol 2008; 70(3): 910-949.

[7]. Katsnelson LB, Vikulova NA, Kursanov AG, et al. Electro-mechanical coupling in a one-dimensional model of heart muscle fiber. Russ J Numer Anal Math Modelling 2014; 29(5):275–284.

[8]. Jahnke T, Lubich C. Error bounds for exponential operator splittings. BIT Numerical Mathematics 2000; 40:735-744.

[9]. Zygmunt AC, Eddlestone GT, Thomas GP, et al. Larger late sodium conductance in M cells contributes to electrical heterogeneity in canine ventricle. Am J Physiol Heart Circ Physiol 2001; 281:H689-697.

[10]. Franz MR, Bargheer K, Rafflenbeul W, et al. Monophasic action potential mapping in human subjects with normal electrocardiograms: Direct evidence for the genesis of the T wave. Circulation 1987; 75:379–386.

[11]. Antzelevitch C. Ionic, molecular, and cellular bases of QT-interval prolongation and torsade de pointes. Europace 2007; 9(suppl 4):iv4-15.

Address for correspondence.

Nathalie Vikulova (n.vikulova@iip.uran.ru)
Institute of Immunology and Physiology, Ural Branch of the Russian Academy of Sciences, Pervomayskaya st., 106, 620041, Yekaterinburg, Russian Federation